DOI: 10.13009/EUCASS2023-741
Aerospace Europe Conference 2023 – 10TH EUCASS – 9TH CEAS

Filtering techniques assessment towards pose estimation enhancement for image-based proximity navigation with uncooperative space objects.

Gaia Letizia Civardi[⋆†] *and Michele Roberta Lavagna*[⋆]
[⋆]*Politecnico di Milano*
Via La Masa, 34 Milano, Italy
gaialetizia.civardi@polimi.it · michelle.lavagna@polimi.it
[†]Corresponding author

Abstract

Autonomous relative navigation nearby uncooperative space objects represents a hot spot within the space engineering community. One common solution to the problem of determining a spacecraft's pose is to use vision-based navigation techniques. This paper explores the potential benefits of using filtering methods downstream of a vision-based pose determination pipeline to improve its accuracy. Specifically, we adopt a loosely coupled approach that utilizes two distinct filters; one for relative rotational dynamics and another for translational dynamics. The primary objective of this work is to evaluate the most suitable filtering schemes to complement image processing algorithms. To achieve this, we compare the performance of a traditional Extended Kalman Filter against an H_∞ filter that leverages the Yamanaka-Ankersen state transition matrix for relative position estimation. In terms of relative attitude estimation, we compare a nonlinear filter and an observer on the Special Orthogonal group with the well-known multiplicative Extended Kalman Filter. Through a simulation study, we assess and compare the different approaches using direct image processing output as measurements for the filters.

1. Introduction

Missions involving close approaches with uncooperative space objects have become more frequent. These missions encompass tasks such as active debris removal, on-orbit monitoring, and close proximity approaches to small celestial bodies. For instance, the ESA e.Inspector project, currently in phase-B, aims at developing a CubeSat mission to inspect a debris in preparation for its removal.[24] As a result of these advancements, there is an increasing demand for robust and dependable algorithms to estimate the relative state between a spacecraft and a target object directly on-board.[27] Over the past few decades, considerable research has focused on determining the absolute position and attitude (pose), leading to the development of several algorithms. By leveraging Global Navigation Satellite System (GNSS), Inertial Measurement Unit (IMU), and star sensor observations, precise determination of absolute pose can be achieved.[10] However, when it comes to estimating the relative pose with respect to an uncooperative object, these measurements are typically unavailable. In such scenarios, the inertia properties of the target object may not be fully known, and its angular rate can only be roughly estimated using optical-flow techniques. These inherent challenges have a significant impact on the accuracy of the estimates, necessitating the adoption of alternative navigation strategies. In recent years, a wide range of vision-based navigation algorithms for relative pose estimation has been extensively investigated.[17] These approaches can be classified into two primary categories: tightly coupled methods and loosely coupled ones. In a tightly coupled navigation scheme, the image feature points are directly processed within the navigation filter, which incorporates both translational and rotational dynamics into its state.[21] Among these approaches, Simultaneous Localization and Mapping (SLAM) techniques have been thoroughly researched.[26] Conversely, when there is at least a rough geometric model of the target object, model-matching Image Processing (IP) algorithms are preferable. These techniques leverage the knowledge of the target object's 3D geometry to estimate the relative pose by optimizing the matches between keypoints in an image and the topological features of the target object[23,4] . However, the direct output of IP algorithms may not provide highly accurate results, which can introduce significant errors and error drift in the estimation of the relative pose. Therefore, it is crucial to incorporate a filtering block downstream of the IP stage to address these challenges. In space applications, the Kalman Filter (KF) and Extended Kalman Filter (EKF) are the standard approaches utilized to mitigate these issues. These algorithms have been widely employed with different

DOI: 10.13009/EUCASS2023-741

sensor architectures,[9] hoewever their performance decrease with non-nominal tuning and non-Gaussianly distributed measurement noise. Consequently, it is essential to assess the performance of these algorithms when dealing with realistic IP output and explore alternative filtering solutions that do not rely on such restrictive assumptions. In the work of by Pesce et al.,[18] a comparison of filtering techniques for relative attitude estimation is presented. However, the nonlinear estimators are tested against synthetically generated Gaussian measurements, rather than direct IP output, thus restricting the validity of the presented results to an ideal scenario. Our work takes a significant step towards the implementation of an end-to-end relative navigation system by utilizing the direct output of the IP algorithm to evaluate the performance of various filtering schemes. To ensure broad applicability, this work does not delve into a detailed description of the vision-based algorithm but instead presents a concise overview. It is worth underlying that the developed IP chain outputs relative pose measurements in terms of a relative tranlsation vector and a relative rotation matrix, which are then processed by the two filtering blocks. The main contribution and advancements of this work are:

- Formulation of a visual-based navigation chain for relative pose estimation.
- Adaptation of classical and recent filtering techniques for relative pose estimation.
- Investigation of the robustness of the proposed filtering techniques against non-ideal measurements.

The remainder of the paper is organized as follows. Sec. 2 briefly introduces the vision-based navigation chain which is used to generate measurements. Sec. 3 presents the models and the filters for relative position estimation, while the relative attitude estimation task is described sec. 4. In sec. 5 the simulation scenario is illustrated along with all the different test cases analyzed. Qualitative and quantitative analyses are reported. In sec. 6 conclusions are drawn, together with some suggestion for future improvements.

2. Relative navigation architecture

Even though this paper is mainly concerned with the performances of the filtering algorithms, a brief overview of the IP chain is here provided. The IP workflow is depicted in 1

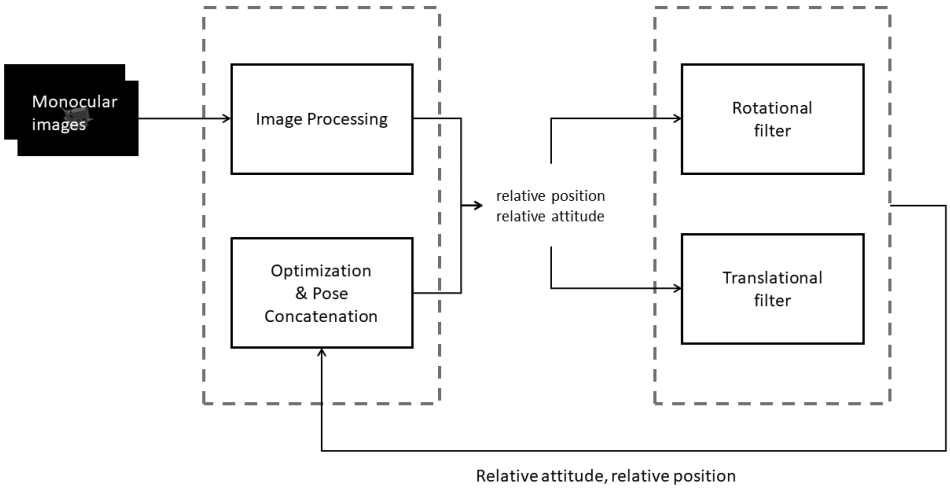

Figure 1: Relative navigation architecture: block diagram

An initial relative pose estimate is assumed to be available, which can be obtained as explained in the work of Bechini et. al.[1] exploiting a coarse model of the target object. Features are then extracted for each image and matched across a consecutive image pair. The correspondences between feature points are then employed to recover the relative pose between two adjacent camera frames, for example solving the Perspective-n-Point Problem (PnP).[8] However, in our test case scenarios, the relative translation vector obtained through the solution of the PnP problem was too inaccurate. Therefore, the relative translation vector expressed in the chaser's camera frame is directly computed from the region of interest (ROI) extracted in the image. To obtain the relative translation vector in the Local Vertical Local Horizon (LVLH) frame, a rotation is performed, accounting for uncertainties in the absolute orbital determination. In particular,

DOI: 10.13009/EUCASS2023-741

the associated noise level is described by a Gaussian distribution with standard deviation $\sigma_{pos} = 1e-02$ km and $\sigma_{vel} = 1e-04$ km/s. As for the rotation measurements, the PnP outputs the relative pose between two consecutive frames, and thus the relative chaser-target rotation matrix can be obtained as:

$$R_k = R_{k-1}A_{rel} \tag{1}$$

where A_{rel} is the relative rotation matrix between two consecutive frames, k and $k-1$ represent two consecutive iteration steps of the navigation filter. Finally, an optimization step is performed to refine the coarse pose estimated. Please notice that in this way, only the relative rotation measurements are correlated with the previous estimate, while the relative translational ones are totally uncorrelated from one another and from the relative rotation estimate.

3. Relative translation

This section is concerned with the models and filters adopted for the description of the relative position. First, the coordinate system adopted in the work is described, and then the two filtering algorithms are presented.

3.1 Coordinate system

The relative position between a *chaser* spacecraft and an uncooperative *target* is described with respect to a local-vertical local-horizontal (LVLH) frame attached to the chaser; with x being a unitary norm vector the chaser's radial direction, z is the component in the direction of the chaser's orbital angular momentum, and y is the component along the direction completing the right-handed orthogonal triad.

3.2 Extended Kalman Filter

Considering a generic non-linear system

$$\begin{aligned} \dot{\mathbf{x}} &= f(\mathbf{x}, t) + G(\mathbf{x})\boldsymbol{w} \\ \mathbf{y} &= h(\mathbf{X}, t) + \boldsymbol{v} \end{aligned} \tag{2}$$

Where f is a non-linear function, $\mathbf{w}$ is a zero-mean, Gaussian process noise with known covariance Q and G is a noise mapping function. The system output is linked to the current state $\mathbf{x}$ by a generic function h, while $\mathbf{v}$ is a zero-mean, Gaussian process noise with known standard deviation. The EKF routine is summarized in Table 1, in which Q is the process covariance matrix, R is the measurement covariance matrix and $\mathbf{F}$, $\mathbf{H}$ are the jacobian matrices of $f(\mathbf{x}, t)$ and $h(\mathbf{x}, t)$, respectively. The only exception to the traditional EKF scheme is the *posterior covariance* update, which is computed following the *Joseph's Formula* for stability reasons.[20]

Algorithm 1 Extended Kalman Filter

Initialization:

$\hat{\mathbf{x}}(t_0) = \mathbf{x}(t_0)$

$P(t_0) = P_0$

Filtering:

$\hat{\mathbf{x}}_k^- = \int_{t_{k-1}}^{t_k} f(\mathbf{x}(\tau))d\tau$

$P_k^- = \Phi(t_k, t_{k-1})P_{k-1}^+\Phi^T(t_k, t_{k-1}) + GQG^T\Delta t$

$K_k = P_k^- H_k^T(H_k P_k^- H_k^T + R_k)^{-1}$

$\hat{x}_k^+ = \hat{\mathbf{x}}_k^- + K_k(\mathbf{y}_k - h(\hat{\mathbf{x}}_k^-))$

$P_k^+ = (I - K_k H_k)P_k^-(I - K_k H_k)^T + K_k R K_k^T$

Where Φ is the state transition matrix, that can be approximated with a series expansion:

$$\Phi(t, t_0) = I + F_t\Delta t + F_t^2\frac{\Delta t^2}{2} + F_t^3\frac{\Delta t^3}{3!} + \cdots \tag{3}$$

DOI: 10.13009/EUCASS2023-741

Our EKF adopts an unperturbed non-linear relative translational model. The free-evolving trajectory of the target in the chaser's LVLH reference frame is described by the following set of differential equations:[22]

$$\begin{aligned} \ddot{x} - 2\dot{\theta}_C\dot{y} - \ddot{\theta}_C y - \dot{\theta}_C^2 x &= \frac{\mu(r_C + x)}{[(r_C + x)^2 + y^2 + z^2]^{3/2}} + \frac{\mu}{r_C^2} \\ \ddot{y} + 2\dot{\theta}_C\dot{x} + \ddot{\theta}_C x - \dot{\theta}_C^2 y &= \frac{\mu y}{[(r_C + x)^2 + y^2 + z^2]^{3/2}} \\ \ddot{z} &= \frac{\mu z}{[(r_C + x)^2 + y^2 + z^2]^{3/2}} \end{aligned} \tag{4}$$

In which $[x, y, z]$ is the relative position vector in the LVLH frame, r_C is the chaser orbital position magnitude, θ_C is the chaser true anomaly and μ is the Earth's gravitational constant. An unperturbed motion model is considered mainly because of the short duration of vision-based proximity operations. Please note that in our case, there is no need to compute the measurement Jacobian, as the IP pipeline directly provides the relative position, which is linearly connected to the state vector.

3.3 H_∞ Filter

The standard Kalman filter is an optimal estimator for linear systems with zero-mean Gaussian process and measurement noise. However, when dealing with the output of an image processing chain that may contain nonlinearities and outliers, the assumptions of the Kalman filter may not be met. A robust counterpart of the KF is the H_∞ filter, which minimizes the ∞-norm of the estimation error without relying on restrictive assumptions regarding the statistics of the process and measurement noise.[25] Let's consider a linear time-invariant system:

$$\begin{aligned} \boldsymbol{x}_{k+1} &= F\boldsymbol{x}_k + G\boldsymbol{w}_k \\ \boldsymbol{y}_k &= H\boldsymbol{x}_k + \boldsymbol{v}_k \end{aligned} \tag{5}$$

with $\boldsymbol{x}_k$ being the state vector, $\boldsymbol{w}_k$ and $\boldsymbol{v}_k$ the process and measurement noise respectively with associated covariance matrices Q and R, similarly to the EKF. The routine of the H_∞ is similar to the EKF one , with the main difference being the computation of the gain matrix K_k. In particular, K_k is chosen such that $\|\boldsymbol{x} - \hat{\boldsymbol{x}}\|_\infty < \frac{1}{\gamma}$, where $\boldsymbol{x}$ and $\hat{\boldsymbol{x}}$ represent the true and predicted state, respectively and γ is the tuning parameter. The complete formulation of the H_∞ filter is reported in Table 2.

Algorithm 2 H_∞ filter

Initialization:

$\hat{\mathbf{x}}(t_0) = \mathbf{x}(t_0)$

$P(t_0) = P_0$

Filtering:

$K_k = P_k[I - \gamma P_k + H_k^T R_k^{-1} H_k P_k]^{-1} H_k^T R_k^{-1}$

$\hat{\mathbf{x}}_{k+1} = F_k\hat{\mathbf{x}}_k + F_k K_k(\mathbf{y}_k - H_k\hat{\mathbf{x}}_k)$

$P_{k+1} = F_k P_k(I - \gamma P_k + H_k^T R_k^{-1} H_k P_k)^{-1} F_k^T + Q_k$

The H_∞ requires the adoption of a linear motion formulation. In our work, we use the model developed by Yamanaka and Ankersen,[28] which is a linearised formulation for arbitrary elliptical orbits. A brief description of the model is presented hereafter. First, a set of modified coordinates is obtained from the relative position $\boldsymbol{r}$ and velocity $\boldsymbol{v}$ vectors expressed in the LVLH frame:

$$\begin{aligned} \tilde{\boldsymbol{r}} &= \rho\boldsymbol{r} \\ \tilde{\boldsymbol{v}} &= e\sin\theta\boldsymbol{r} + (1/k^2\rho)\boldsymbol{v} \end{aligned} \tag{6}$$

Then, a set of pseudoinitial conditions for the propagation of the in-plane components can be computed from the modified coordinates as:

$$\begin{bmatrix} \bar{x}_0 \\ \bar{y}_0 \\ \dot{\bar{x}}_0 \\ \dot{\bar{y}}_0 \end{bmatrix} = \frac{1}{1-e^2} \begin{bmatrix} -3s(\frac{1}{\rho} + \frac{e^2}{\rho^2}) & 0 & c - 2e & -s(1 + \frac{1}{\rho}) \\ -3es(\frac{1}{\rho} + \frac{1}{\rho^2}) & 1 - e^2 & ec - 2 & -es(1 + \frac{1}{\rho}) \\ -1 + e^2 + 3\rho & 0 & es & \rho^2 \\ 3(\frac{c}{\rho} + e) & 0 & s & c(1 + \frac{1}{\rho}) + e \end{bmatrix} \begin{bmatrix} \tilde{x} \\ \tilde{y} \\ \dot{\tilde{x}} \\ \dot{\tilde{y}} \end{bmatrix} \tag{7}$$

DOI: 10.13009/EUCASS2023-741

Once the pseudoinitial values have been obtained, the relative in-plane components can be calculated as follows:

$$\begin{bmatrix} \dot{\bar{x}} \\ \dot{\bar{y}} \\ \ddot{\bar{x}} \\ \ddot{\bar{y}} \end{bmatrix} = \begin{bmatrix} s & 0 & (2-3esJ) & -c \\ c(1+\frac{1}{\rho}) & 1 & -3\rho^2 J & s(1+\frac{1}{\rho}) \\ s' & 0 & -3e(s'J+\frac{s}{\rho^2}) & -c' \\ -2s & 0 & -3(1-2esJ) & 2c-e \end{bmatrix}_{\theta} \begin{bmatrix} \bar{x}_0 \\ \bar{y}_0 \\ \dot{\bar{x}}_0 \\ \dot{\bar{y}}_0 \end{bmatrix} \tag{8}$$

while the relative state for the out-of-plane component can be obtained as:

$$\begin{bmatrix} \tilde{z} \\ \dot{\tilde{z}} \end{bmatrix} = \frac{1}{\rho_{\theta-\theta_0}} \begin{bmatrix} c & s \\ -s & c \end{bmatrix}_{\theta-\theta_0} \begin{bmatrix} \tilde{z} \\ \dot{\tilde{z}} \end{bmatrix} \tag{9}$$

where

$$\begin{aligned} \rho &= 1 + e\cos\theta \\ s &= \rho\cos\theta \\ c &= \rho\sin\theta \\ s' &= \cos\theta + e\cos 2\theta \\ c' &= -(\sin\theta + e\sin 2\theta) \\ J &= k^2(t-t_0) \\ k^2 &= h/p^2 \end{aligned} \tag{10}$$

with e being the chaser's eccentricity, θ, chaser's true anomaly and $|_\theta$ meaning evaluated at the true anomaly θ at the current time step. It is worth underlying that the YA motion model may be sensitive to errors in the absolute orbital determination, and thus is it important to evaluate such effects within our test case scenarios.

4. Relative rotation

The following section is concerned with the description of the models and the filters for relative attitude estimation.

4.1 Coordinate system and attitude kinematics

The attitude of a rigid body naturally evolves on the Special Orthogonal Group *SO(3)*, that is the set of 3×3 orthonormal matrices. The Lie algebra of *SO(3)* is represented by the set of 3×3 skew-symmetric matrices and it is generally denoted as *so(3)*. The relative attitude kinematics between two rigid bodies can be written as:

$$\dot{R} = R(\boldsymbol{\omega})_\times, \quad R(0) = R_0 \tag{11}$$

where $R(t) \in SO(3)$ is the relative rotation matrix which represents the attitude of the target object with respect to the chaser spacecraft, expressed in the chaser body frame and $\boldsymbol{\omega}$ is the relative angular velocity expressed in the chaser frame. Attitude kinematics can also be expressed using the quaternion representation of the attitude. The unit quaternion is a four-dimensional vector, which can be defined in terms of Euler axis $\boldsymbol{e}$ and rotation angle θ as follows:

$$\mathbf{q} = \begin{bmatrix} \boldsymbol{\rho} \\ q_4 \end{bmatrix} \tag{12}$$

where

$$\boldsymbol{\rho} = \begin{bmatrix} q_1 & q_2 & q_3 \end{bmatrix} = \boldsymbol{e}\sin(\theta/2) \tag{13}$$

and

$$q_4 = \cos(\theta/2) \tag{14}$$

The quaternion always obeys the unit-norm constraint. In this work, we adopt $\mathbf{q}$ to represent the relative attitude. The kinematics of the quaternion reads:

$$\dot{\mathbf{q}} = \frac{1}{2}\Omega(\boldsymbol{\omega})\mathbf{q} = \frac{1}{2}\Xi(\mathbf{q})\boldsymbol{\omega} \tag{15}$$

where

$$\Omega(\boldsymbol{\omega}) = \begin{bmatrix} 0 & \omega_z & -\omega_y & \omega_x \\ -\omega_z & 0 & \omega_x & \omega_y \\ \omega_y & -\omega_x & 0 & \omega_z \\ -\omega_x & -\omega_y & -\omega_z & 0 \end{bmatrix} \tag{16}$$

Where $\boldsymbol{\omega}$ is again the relative angular velocity expressed in the chaser body frame. The relative attitude dynamics is not here presented, since all the proposed algorithms are kinematics-only filters.

DOI: 10.13009/EUCASS2023-741

4.1.1 Augmented Multiplicative Extended Kalman Filter (AMEKF)

The Multiplicative Extended Kalman Filter (MEKF), which is based on a local linearization of the attitude around the current state estimate, has been widely employed for on-board attitude estimation. The MEKF uses the quaternion as a global attitude representation and it uses a three-component state vector for the local representation of attitude errors. Our implementation differs from classical one[11] due to the fact that the angular acceleration of the target is not known. Thus, the relative angular velocity has been added to the state vector, and it is assumed to be constant[5] up to a process disturbance $B\boldsymbol{w}$:

$$\dot{\boldsymbol{\omega}} = \mathbf{0} + B\boldsymbol{w} \tag{17}$$

where $\boldsymbol{w}$ is a zero-mean Gaussian noise process with given covariance Q. This is a reasonable assumption if no prior information about the angular rates of the target object is available and if the relative angular rate is small enough to be approximated as constant the integration time step of the navigation filter. The measurement equation is given by:

$$\boldsymbol{y} = h(\boldsymbol{q}) + D\boldsymbol{v} \tag{18}$$

where $h(\boldsymbol{q})$ is the noise-free vector of measurements, and $\boldsymbol{v}$ is a vector of zero-mean Gaussian noise processes with covariance R. Since our IP chain directly estimates the relative rotation matrix, the measurement function is written as:

$$h(\boldsymbol{q}) = \begin{bmatrix} A(\boldsymbol{q})\bar{\boldsymbol{r}}_1 \\ A(\boldsymbol{q})\bar{\boldsymbol{r}}_2 \end{bmatrix} \tag{19}$$

in which $A(\boldsymbol{q})$ is the relative attitude matrix, $\bar{\boldsymbol{r}}_1$ and $\bar{\boldsymbol{r}}_2$ are two mutually orthogonal reference directions. The AMEKF is summarized in Table 3.

Algorithm 3 Augmented Multiplicative Extendend Kalman Filter

Initialization:

$\hat{\boldsymbol{q}}(t_0) = \hat{\boldsymbol{q}}_0$

$\hat{\boldsymbol{\omega}}(t_0) = \hat{\boldsymbol{\omega}}_0$

$P(t_0) = P_0$

Prediction:

$\dot{\hat{\boldsymbol{q}}} = \frac{1}{2}\Omega(\hat{\boldsymbol{\omega}})\hat{\boldsymbol{q}}$

$\dot{\hat{\boldsymbol{\omega}}} = \mathbf{0}$

$P_k^- = \Phi(t_k, t_{k-1})P_{k-1}^+\Phi^T(t_k, t_{k-1}) + BQB^T\Delta t$

where

$F(t) = \begin{bmatrix} -\hat{\omega}_\times & I_{3\times3} \\ 0_{3\times3} & 0_{3\times3} \end{bmatrix}$

$\Phi = I + F\Delta t$

$G = \begin{bmatrix} 0_{3\times3} & I_{3\times3} \end{bmatrix}^T$

$Q = \sigma_w^2 I_{3\times3}$

Correction

$K_k = P_k^- H_k^T(H_k P_k^- H_k^T + R_k)^{-1}$

$R = \sigma_v^2 I_{3\times3}$

$P_k^+ = (I - K_k H_k)P_k^-(I - K_k H_k)^T + K_k R K_k^T$

$\hat{\boldsymbol{q}}_k^+ = \hat{\boldsymbol{q}}_k^- + \frac{1}{2}\Xi(\hat{\boldsymbol{q}}_k^-)K_k[y_k - h(\hat{\boldsymbol{q}}_k^-)]$

4.1.2 Second Order Minimum Energy Filter on *SO(3)*

Minimum Energy Filtering represents a determinstc alternative to the stochastic MEKF. It was first introduced by Mortensen[13] and later applied to attitude estimation on SO(3) by Zamani.[29] The first application of the Second Order Minimum Energy Filter for relative attitude estimation can be found in the work of Pesce,[19] in which this novel estimator outperforms the classical MEKF. Building on these results, we employ a formulation which is solely based on the kinematic model, which does not require knowledge of the target's inertia matrix. Although a filter that incorporates

DOI: 10.13009/EUCASS2023-741

relative attitude dynamics may outperform it, the mentioned model is still valuable as it can handle partially unknown objects. This capability is particularly desirable when dealing with derelict targets like space debris. In particular:

$$\dot{R} = R(\omega(t))_\times \tag{20}$$

While the relative angular velocity is assumed to be constant up to white noise, as previously done for the AMEKF:

$$\dot{\boldsymbol{\omega}} = B\boldsymbol{w} \tag{21}$$

Equations 20 and 21 already represent the evolution of the relative rotation matrix and relative angular velocity, respectively, and they do not rely on the dynamics equations. The complete formulation of the kinematic second-order minimun energy filter is summarized below in Table 4, assuming the same measurement input as the AMEKF.

Algorithm 4 Second Order Kinematic Minimum Energy Filter on SO(3)

Initialization:

$\hat{R(t_0)} = \hat{R}_0$

$\hat{\omega(t_0)} = \hat{\omega}_0$

$K(t_0) = K_0$

Main Filtering Step:

$\dot{\hat{R}} = \hat{R}\left(\hat{\omega(t)} + K_{11}\boldsymbol{r}^R + K_{12}\boldsymbol{r}^\omega\right)_\times$

$\dot{\hat{\omega}} = K_{21}\boldsymbol{r}^R + K_{22}\boldsymbol{r}^\omega$

$\dot{K}(t) = -\alpha K + AK + KA^T - KEK + BR^{-1}B^T - WK - KW^T$

where

$\boldsymbol{r}^t = \begin{bmatrix} \boldsymbol{r}^R \\ \boldsymbol{r}^\omega \end{bmatrix} = \begin{bmatrix} u_1(\hat{\boldsymbol{r}_1} \times \boldsymbol{r}_1 - u_2\hat{\boldsymbol{r}_2} \times \boldsymbol{r}_2) \\ \mathbf{0} \end{bmatrix}$

$u_i = b^2/d_i^2$

$\hat{\boldsymbol{r}_i} = \hat{R}^T\bar{r}_i, \quad \boldsymbol{r}_i = R^T\bar{r}_i + d_i\boldsymbol{\epsilon}$

In which K is the six-by-six gain matrix, b and d_i model the process and measurement noise, respectively and α is a forgetting factor for the integration of the matrix riccati equation of the gain. It is worth mentioning that the full state of the second order minimum energy filter is a 48-by-1 vector, and thus it may be computationally demanding for an on-board implementation.

4.1.3 Equivariant Observer on *SE(3)*

The Lie-group *SE(3)* is usually considered a model for rigid-body transformations of the Euclidean space. It has been recently shown[15] that this group can also be used to model a symmetry of the second-order velocity kinematics for attitude. In their recent work, Ng et. al.[14] demonstrate that the second order kinematics are equivariant, and then derive a second-order observer on the *SE(3)* group. We propose and adaptation of their observer to the case of relative attitude estimation, in which measurements of the relative angular velocity are not available. The complete derivation of the observer is here omitted for brevity, and only the key concepts are reported. A generic element of the Special Euclidean group *SE(3)* can be written as follows:

$$SE(3) = \{(Q, q) | Q \in SO(3), q \in R^3\} \tag{22}$$

It is then necessary to define the product manifold:

$$\mathcal{M} = SO(3) \times so(3) \tag{23}$$

and a group action $\Phi : SE(3) \times \mathcal{M} \to \mathcal{M}$ is defined as:

$$\Phi((Q, q), (R, \omega_\times)) = (RQ, (Q^T(\omega + q))^\times) \tag{24}$$

DOI: 10.13009/EUCASS2023-741

Let (R_0, ω_0) be a constant reference state in $\mathcal{M}$ and let $\hat{X} = (\hat{Q}, \hat{q}) \in SE(3)$, with arbitrary initial conditions $\hat{X(0)} = (\hat{Q}(0), \hat{q}(0))$. The observer state can be obtained as:

$$(\hat{Q}, \hat{q}) = \Phi\Big(((\hat{R}, \hat{\omega}), (R_0, \omega_0))\Big) \tag{25}$$

In which $\hat{R}, \hat{\omega}$ represent the relative rotation and relative angular velocity estimates. The formulation of the second-order equivariant observer is reported in Table 5. The same measurement model as before is employed, and the input angular acceleration is assumed to be null.

Algorithm 5 Second Order Equivariant Observer

Initialisation:

$\hat{Q(t_0)} = \hat{Q}_0$

$\hat{q(t_0)} = \hat{q}_0$

Main Filtering Step:

$\dot{\hat{Q}} = (\omega_0 + \hat{q})_\times \hat{Q} + (\hat{Q}\hat{\pi})_\times \hat{Q}$

$\dot{\hat{q}} = (\hat{Q}\hat{\pi})_\times (\omega_0 + \hat{q}) + \hat{Q}\hat{\theta}$

where

$\hat{\pi} = k_1(\boldsymbol{r}_1 \times \hat{Q}^T R_0^T \bar{\boldsymbol{r}}_1 + \boldsymbol{r}_2 \times \hat{Q}^T R_0^T \bar{\boldsymbol{r}}_2)$

$\hat{\theta} = k_2(\boldsymbol{r}_1 \times \hat{Q}^T R_0^T \bar{\boldsymbol{r}}_1 + \boldsymbol{r}_2 \times \hat{Q}^T R_0^T \bar{\boldsymbol{r}}_2)$

$\boldsymbol{r}_i = R^T \bar{r}_i + d_i \boldsymbol{\epsilon}$

With k_1, k_2 being two scalar gains. In our formulation we set R_0, ω_0 to be a random orthonormal matrix and a random three-by-one vector. It is important to highlight that while a fixed-gain observer is not an optimal estimator, it has the advantage of being immune to the instabilities commonly associated with the numerical integration of the matrix Riccati equation. Additionally, the computational burden of a fixed-gain observer is significantly lighter compared to the Second Order Minimum Energy filter, as the latter necessitates the integration of the six-by-six gain matrix during each observation step.

5. Simulations and results

In this section, the numerical simulation environment to test the different filtering formulations is described. The IP chain is briefly illustrated and the different simulation scenarios are presented. An overview of the results is provided, with a critical discussion of the filtering schemes' performances.

5.1 Simulation Scenario Description

The relative navigation architecture is preliminarily tested on synthetically generated images of the Tango spacecraft,[2] adopting the same camera properties as the one employed for SPEED datasets[16,6]. The reference orbital and attitude dynamics for the two spacecrafts are integrated directly in the Earth Centered Inertial (ECI) frame, accounting for the Earth oblateness effect, solar radiation pressure and drag perturbations. It is worth noticing that the chaser's attitude is controlled in order to keep the target in the camera's field of View (FOV). The target orbital parameters are reported in table 1.

Table 1: Scenario orbital parameters

Parameter	Value
a [km]	7120.9
e [-]	4.2e-03
i [deg]	98.2
Ω [deg]	45
ω [deg]	70

DOI: 10.13009/EUCASS2023-741

The target inertia properties have been derived considering a uniform mass distribution and assuming that the target body frame coincides with the principal axis of inertia. The resulting inertia matrix is thus:

$$I_{tango} = \begin{bmatrix} 2.38 & 0 & 0 \\ 0 & 2.13 & 0 \\ 0 & 0 & 3.86 \end{bmatrix} kgm^2 \tag{26}$$

The generated relative trajectory is used both to evaluate the relative navigation algorithm performances and to provide input to the image generation tool. The details of the image rendering tool used in this work can be found in a previous work of the author[3] and thus they will not be discussed further. The main driver for the different scenarios is represented by the target's angular velocity. In fact, it is directly linked to the performances of the relative rotation filters and to the effectiveness of the IP chain. For this reason, different cases are introduced, with the angular rate of the target that ranges from a low value up to an almost tumbling motion. Further, two different orbital scenarios are considered, according to the relative distance w.r.t. the target object. In the first case, the object occupies a large percentage of the camera FOV (Figure 2a), while in the second case, the target object only occupies a small part of the FOV (Figure 2b), thus representing a higher challenge for the IP. The specifications of the different test cases are summarized in Table. 2.

Table 2: Specifications of the test cases.

Cases	Number of runs	Inital attitude error [deg]	Initial position error [m]	Target's angular velocity [deg/s]	Relative range [m]
A1	100	α, β, γ $\in$ [-8, 8]	x, y, z $\in$ [-1.2, 1.2]	[-0.8, 0.5, 0.2]	6
A2	100	α, β, γ $\in$ [-8, 8]	x, y, z $\in$ [-1.2, 1.2]	[-1.8, 2.5, 1.2]	6
A3	100	α, β, γ $\in$ [-8, 8]	x, y, z $\in$ [-1.2, 1.2]	[-1.8, 3.5, 2.2]	6
B1	100	α, β, γ $\in$ [-8, 8]	x, y, z $\in$ [-3.5, 3.5]	[-0.8, 0.5, 0.2]	16.5
B2	100	α, β, γ $\in$ [-8, 8]	x, y, z $\in$ [-3.5, 3.5]	[-1.8, 2.5, 1.2]	16.5
B3	100	α, β, γ $\in$ [-8, 8]	x, y, z $\in$ [-3.5, 3.5]	[-1.8, 3.5, 2.2]	16.5

Concerning the filters' initialisation, the initial attitude is constructed considering a deviation from the true attitude that is uniformly drawn from ([-8, 8] deg) on each axis; while the translational filters are initialized with a uniform error distribution up to 20% of the true inter-satellite distance and 2% of the relative velocity. The filters are run at 1Hz, which is compatible with the execution time of the IP algorithms.

(a) Small inter-satellite distance

(b) High inter-satellite distance

Figure 2: Source images for the vision-based navigation chain

The EKF and H_∞ are set with $Q_{pos} = (1e-03)^2$, $Q_{vel} = (1e-04)^2$ to model the position and velocity process noise, respectively. The measurement covariance matrix is instead $R = (0.5e-02)^2 I_3$ for the test case A and $R = (1.5e-02)^2 I_3$ for the test case B. The AMEKF is tuned with $Q = (1e-02)^2 I3$, and $R = (3.e-02)^2 I_3$, respectively. The second order kinematic filter is tuned with $K = 5I_6$, $\alpha = 1e-03$; while the observer gains are set to $k1 = 0.8$, $k_2 = 0.008$

DOI: 10.13009/EUCASS2023-741

respectively. It is important to stress the fact that these tuning parameters were found to give good performances in terms of stability and steady-state performance across different scenarios; while it would be necessary to carry out a specific tuning campaign to find the best tuning parameters for each test case scenario.

5.2 Results

The relative position error is defined as:

$$e_\rho = \sqrt{(x_i - \hat{x}_i)^2 + (y_i - \hat{y}_i)^2 + (z_i - \hat{z}_i)^2} \tag{27}$$

where $\hat{x}$, $\hat{y}$, $\hat{z}$ are the position components estimates. The relative attitude error is computed following the approach of Markley et. al:[12]

$$e_R = arccos\left(1 - \frac{tr(I - R^T\hat{R})}{2}\right) \tag{28}$$

with $\hat{R}$ being the estimated rotation matrix. Figure 3 illustrates the relative attitude and position errors, calculated using Equations (27) and (28), for both the minimum energy filter and $H\infty$ filter. The results are averaged over 100 runs for test case A1, alongside the performance of the IP chain. Similarly, fig. 4 presents the results for test case B1, utilizing the EKF and the equivariant observer. From these analyses, several qualitative observations can be made. Firstly, it is crucial to highlight the benefits of incorporating the filter after the IP block, especially concerning the translational part. The estimation error is generally reduced when the filter is integrated, and it prevents the accumulation and drift of errors over time. Error peaks are noticeable in the relative attitude estimation when the IP block produces highly inaccurate results. In such cases, all the rotational filters struggle to mitigate measurement outliers. The sudden increase in measurement error towards the end of test case A1 is attributed to the illumination conditions of the target object, which significantly affects the performance of the whole IP chain. In terms of relative rotation, the filter cannot reduce significantly the input measurements error. This may be due to the fact that the measurements are correlated with one another and that due to the rotation matrix concatenation, the error tends to accumulate. For a more quantitative analysis, Table 3 provides the Root Mean Square Error (RMSE) for all cases. Notably, the AMEKF consistently exhibits the highest estimation error, likely due to the non-Gaussian distribution of measurements. This high error renders it unsuitable for practical applications, emphasizing the need for a more robust alternative. Comparatively, the minimum energy filter and the equivariant observer demonstrate similar performances in terms accuracy, with the latter consistently yielding lower estimation errors. However, it is important to stress the fact that the fixed-gain observer is more sensitive to measurement outliers. As expected, higher relative angular velocity leads to increased attitude estimation error for all rotational filters. This is attributed to the fact that the filter's sample time (1 second) may be too large to accurately approximate the angular velocity as constant. Strategies such as decreasing the filter's sample time or obtaining a reliable estimate of the angular velocity (e.g., using a multiple model filter[7]) can be employed to address this issue. Regarding relative translation results, a higher angular rate proves beneficial for both the IP chain and the filters, resulting in reduced estimation error. Concerning the relative translation, it can be noticed that the estimation error is worse in the small inter-satellite distance case, being around 5% of the relative range, while in the test case B the error remains below the 3%. Finally, it is worth noting that the EKF and H_∞ filter consistently demonstrate similar performance. This can be attributed to the relatively small inter-satellite distance compared to the chaser's orbital radius, allowing the linearized motion model to sufficiently describe the relative position over time.

DOI: 10.13009/EUCASS2023-741

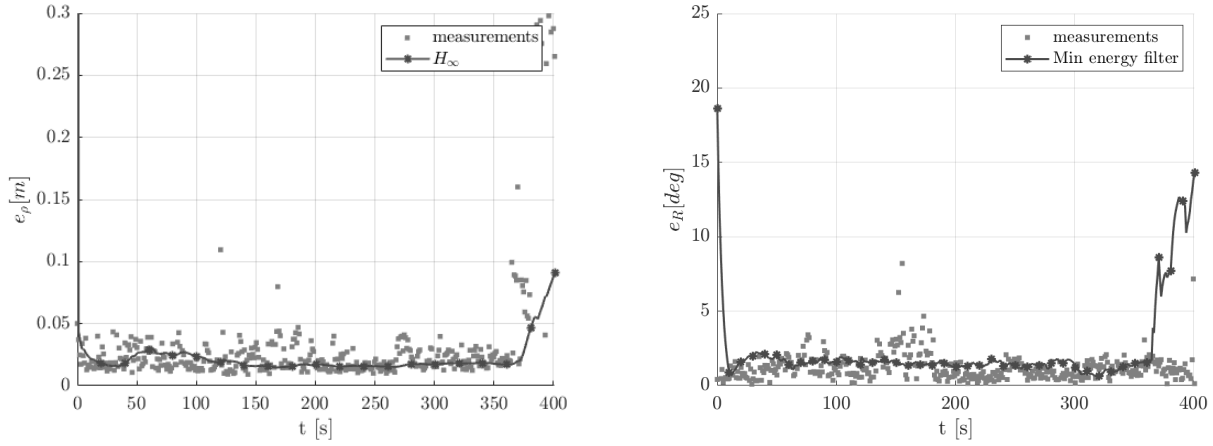

(a) Relative position error

(b) Relative attitude error

Figure 3: Average estimation errors for test case A1 using H_∞ and minimum energy filter.

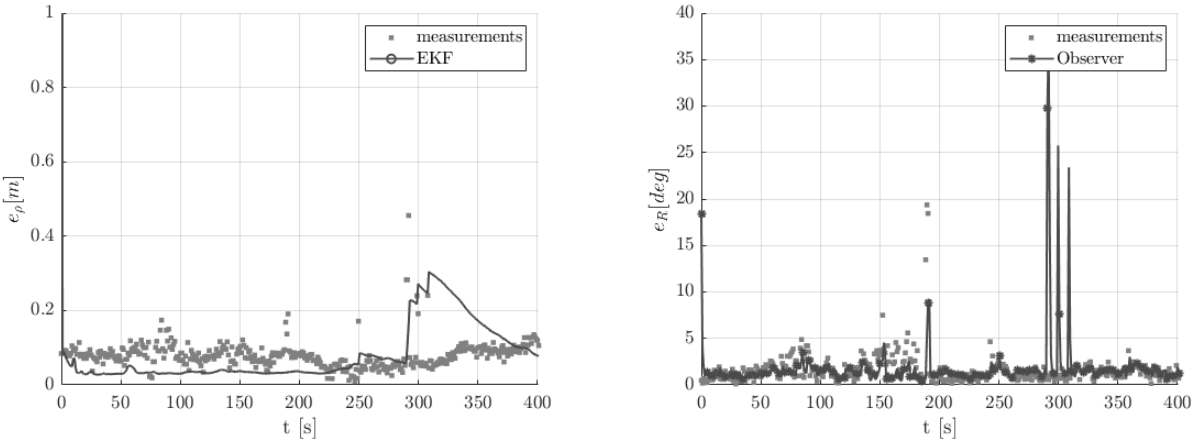

(a) Relative position error

(b) Relative attitude error

Figure 4: Average estimation errors for test case B1 using EKF and Minimum energy filter.

Table 3: Filters RMSE results.

Cases	RMSE - position [m]		RMSE - attitude [deg]		
	H_∞	EKF	AMEKF	Observer	Min. Energy Filter
A1	0.162	0.158	2.135	1.541	1.579
A2	0.168	0.164	2.851	1.903	2.152
A3	0.196	0.166	3.582	3.192	3.410
B1	0.235	0.267	1.876	1.215	1.267
B2	0.445	0.436	2.781	1.975	2.186
B3	0.744	1.071	3.671	3.618	3.778

5.3 Robustness to large initialization error

To assess the robustness of the selected filtering techniques, we replicated test case scenario B1 with additional variations. In this case, we introduced an initial attitude estimation error uniformly distributed within ([-25, 25] deg) for each axis and an initial position error up to 50% of the true inter-satellite distance. The purpose of this analysis is to evaluate the effectiveness of the proposed navigation solution under non-ideal conditions, such as when a significant pose initialization error is present. Figure 5 illustrates the average estimation errors over 50 runs. The AMEKF was

DOI: 10.13009/EUCASS2023-741

excluded from this analysis due to its consistently poor performance across all test cases. The filter settings remained the same as in the previous test cases. The results depicted in Figure 5 indicate that the minimum energy filter exhibits an oscillatory behavior during the transient phase, which corresponds to the convergence of the gain vector towards its steady-state value. As anticipated, this behavior is not observed in the observer, which demonstrates faster convergence to the steady state. However, the observer appears to be more sensitive to measurement outliers compared to the minimum energy filter, due to its fixed gain. Regarding the relative translational component, the H_∞ and the EKF display a similar transient behaviour. Nevertheless, both the H_∞ filter achieve better steady-state performance, especially in terms of robustness with respect to IP outliers. These results suggest that a robust estimator paired with a linearized motion model can be as effective as a more complex algorithm such as the EKF.

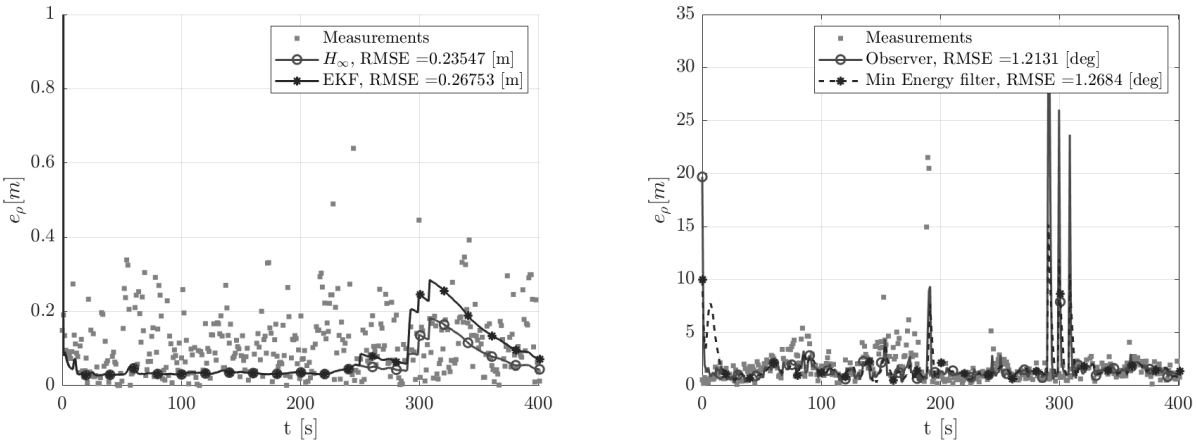

(a) Relative position error

(b) Relative attitude error

Figure 5: Average estimation errors for large initialization errors.

6. Conclusions

The problem of estimating the relative pose for proximity operations with uncooperative targets has been analyzed, and various filtering techniques have been tested for this specific application. Two filtering algorithms, namely the EKF and the H_∞ filter, have been considered for relative position estimation. A comparison was made between the AMEKF, a kinematic second-order filter, and an equivariant observer. A simulation campaign was conducted to evaluate the performance of these filters when using real IP output as measurements. The study also examined the influence of initialization errors and the angular rate of the target on the filter performance. Based on the presented results, it can be concluded that the AMEKF is not robust enough to handle non-Gaussian distributed measurements with significant outliers. Hence, more robust alternatives should be favoured. Both the equivariant observer and the minimum energy filter showed promise, with the former offering computational efficiency. Further, the minimum energy filter exhibited oscillatory behaviour during the transient phase, which may negatively impact the performance of a closed-loop navigation system. The equivariant observer, instead, showed faster convergence to the steady state. Additionally, it was observed that the relative attitude estimation performance of kinematic filters is strongly influenced by the angular velocity of the target. Lastly, it is important to stress the fact that for future development it would be preferable to avoid estimating the relative pose between two adjacent frames since it leads to error accumulation in the rotational states. Regarding relative translation estimation, it can be concluded that for small inter-satellite distances, adopting a linearized motion model can be as effective as using a non-linear model, especially when combined with a robust estimator like the H_∞ filter. Overall, these findings highlight the need for robust estimators to handle non-Gaussian measurements and large initialization errors. The equivariant observer and the minimum energy filter offer promising alternatives, while the H_∞ filter demonstrates robustness and efficiency in relative translation estimation.

References

[1] Michele Bechini, Gaia Letizia Civardi, Matteo Quirino, Alessandro Colombo, and Michéle Lavagna. Robust monocular pose initialization via visual and thermal image fusion. In *73rd International Astronautical Congress (IAC 2022), International Astronautical Federation, IAF, Paris, France*, pages 1–15, 09 2022.

DOI: 10.13009/EUCASS2023-741

[2] Michele Bechini, Michèle Lavagna, and Paolo Lunghi. Dataset generation and validation for spacecraft pose estimation via monocular images processing. *Acta Astronautica*, 204:358–369, 2023.

[3] Gaia Letizia Civardi, Michele Bechini, Matteo Quirino, Alessandro Colombo, Margherita Piccinin, and Michèle Lavagna. Generation of fused visible and thermal-infrared images for uncooperative spacecraft proximity navigation. *Advances in Space Research*, 2023.

[4] Michael Gansmann, Olivier Mongrard, and Finn Ankersen. 3d model-based relative pose estimation for rendezvous and docking using edge features. In *Presentation 10th International ESA Conference on Guidance, Navigation and Control Systems*, pages 1–15, 2017.

[5] Scott Geyer, John Crassidis, Manoranjan Majji, and Roshan Eapen. Relative navigation of uncooperative space bodies. In *AIAA Scitech 2021 Forum*, 01 2021.

[6] Mate Kisantal, Sumant Sharma, Tae Ha Park, Dario Izzo, Marcus Märtens, and Simone D'Amico. Spacecraft pose estimation dataset (speed). *Dataset on Zenodo*, February 2019.

[7] Rahul Kottath, Parag Narkhede, Vipan Kumar, Vinod Karar, and Shashi Poddar. Multiple model adaptive complementary filter for attitude estimation. *Aerospace Science and Technology*, 69:574–581, 2017.

[8] Vincent Lepetit, Francesc Moreno-Noguer, and Pascal Fua. Epnp: An accurate o(n) solution to the pnp problem. *International Journal of Computer Vision*, 81:155–166, 02 2009.

[9] M.D. Lichter and S. Dubowsky. State, shape, and parameter estimation of space objects from range images. In *IEEE International Conference on Robotics and Automation, 2004. Proceedings. ICRA '04. 2004*, volume 3, pages 2974–2979 Vol.3, 2004.

[10] F Landis Markley, John Crassidis, and Yang Cheng. Nonlinear attitude filtering methods. In *AIAA guidance, navigation, and control conference and exhibit*, page 5927, 2005.

[11] F Landis Markley and John L Crassidis. *Fundamentals of spacecraft attitude determination and control*. Space Technology Library. Springer, New York, NY, 2014.

[12] Landis Markley and D. Mortari. Quaternion attitude estimation using vector observations. *Journal of the Astronautical Sciences*, 48, 04 2000.

[13] R. Mortensen. Maximum-likelihood recursive nonlinear filtering. *Journal of Optimization Theory and Applications*, 2:386–394, 11 1968.

[14] Yonhon Ng, Pieter van Goor, Tarek Hamel, and Robert Mahony. Equivariant systems theory and observer design for second order kinematic systems on matrix lie groups. In *2020 59th IEEE Conference on Decision and Control (CDC)*, pages 4194–4199, 2020.

[15] Yonhon Ng, Pieter van Goor, Robert Mahony, and Tarek Hamel. Attitude observation for second order attitude kinematics. In *2019 IEEE 58th Conference on Decision and Control (CDC)*, pages 2536–2542, 2019.

[16] Tae Ha Park, Marcus Märtens, Gurvan Lecuyer, Dario Izzo, and Simone D'Amico. Next Generation Spacecraft Pose Estimation Dataset (SPEED+). *Dataset on Zenodo*, October 2021.

[17] Lorenzo Pasqualetto Cassinis, Robert Fonod, and Eberhard Gill. Review of the robustness and applicability of monocular pose estimation systems for relative navigation with an uncooperative spacecraft. *Progress in Aerospace Sciences*, 06 2019.

[18] Vincenzo Pesce, Muhammad Farooq Haydar, Michele Lavagna, and Marco Lovera. Comparison of filtering techniques for relative attitude estimation of uncooperative space objects. *Aerospace Science and Technology*, 84:318–328, 2019.

[19] Vincenzo Pesce, Roberto Opromolla, Salvatore Sarno, Michèle Lavagna, and Michele Grassi. Autonomous relative navigation around uncooperative spacecraft based on a single camera. *Aerospace Science and Technology*, 84:1070–1080, 2019.

[20] Carpenter J. R. and C. N. D. Souza. Navigation filter best practices. Technical report, NASA, 2018.

DOI: 10.13009/EUCASS2023-741

[21] Shai Segal, Avishy Carmi, and Pini Gurfil. Stereovision-based estimation of relative dynamics between noncooperative satellites: Theory and experiments. *IEEE Transactions on Control Systems Technology*, 22(2):568–584, 2014.

[22] Shay Segal and Pini Gurfil. Effect of kinematic rotation-translation coupling on relative spacecraft translational dynamics. *Journal of Guidance, Control, and Dynamics*, 32(3):1045–1050, 2009.

[23] Jian-Feng Shi, Steve Ulrich, and Stephane Ruel. Spacecraft pose estimation using principal component analysis and a monocular camera. In *AIAA Guidance, Navigation, and Control Conference*, pages 1–24, 2017.

[24] Stefano Silvestrini, Jacopo Prinetto, Giovanni Zanotti, and Michèle Lavagna. Design of robust passively safe relative trajectories for uncooperative debris imaging in preparation to removal. In *AAS/AIAA Astrodynamics Specialist*, 08 2020.

[25] Dan Simon. *Optimal State Estimation*. John Wiley & Sons, Ltd, 2006.

[26] Arne Sonnenburg, Marcel Tkocz, and Klaus Janschek. Ekf-slam based approach for spacecraft rendezvous navigation with unknown target spacecraft. *IFAC Proceedings Volumes*, 43(15):339–344, 2010. 18th IFAC Symposium on Automatic Control in Aerospace.

[27] Joseph A. Starek, Behçet Açıkmeşe, Issa A. Nesnas, and Marco Pavone. Spacecraft autonomy challenges for next-generation space missions. In Eric Feron, editor, *Advances in Control System Technology for Aerospace Applications*, pages 1–48. Springer Berlin Heidelberg, Berlin, Heidelberg, 2016.

[28] Koji Yamanaka and Finn Ankersen. New state transition matrix for relative motion on an arbitrary elliptical orbit. *Journal of Guidance, Control, and Dynamics*, 25(1):60–66, 2002.

[29] Mohammad Zamani, Jochen Trumpf, and Robert Mahony. Minimum-energy filtering for attitude estimation. *Automatic Control, IEEE Transactions on*, 58:2917–2921, 11 2013.